46th Annual Review of Progress
in Quantitative Nondestructive Evaluation
QNDE2019
July 14-19, 2019, Portland, OR, USA

QNDE2019-6949

VOLUMETRIC IMAGING OF DEFECTS THROUGH A NON-PLANAR SURFACE

Jessica G. McKee[1], Rhodri L. T. Bevan, Paul D. Wilcox and Robert E. Malkin
Department of Mechanical Engineering
University of Bristol
Bristol, UK

ABSTRACT

One-dimensional (1D) phased arrays are widely used in NDT industries, but they have numerous limitations due to their element layout. Two-dimensional (2D) phased arrays have yet to become widely deployed in NDE industries, despite the many benefits they bring, such as volumetric imaging from a single array location and the potential for more defect information to be captured. In this work, a sparse 2D phased array is used to accurately image the interior of a specimen with a doubly-curved surface. The array is mechanically scanned across the surface, which is extracted using an imaging algorithm with an absolute error of less than 0.07 mm. The extracted surface is then used to focus within the component and the positioning of defects is investigated using two metrics: the depth above the back wall and the lateral distance from the surface notch. The standard deviation of depth and lateral position measurements of visible defects is 1.16 mm and 0.97 mm respectively.

Keywords: volumetric imaging, 2D phased array, TFM, FMC

NOMENCLATURE

$\boldsymbol{P_1}, \boldsymbol{P_2}$	position vectors of arbitrary imaging points
$\boldsymbol{E_T}, \boldsymbol{E_R}$	position vectors of transmit/receive elements
$\boldsymbol{A}, \boldsymbol{B}$	position vectors of surface-crossing points

1. INTRODUCTION

Ultrasonic phased arrays are commonly used in NDE industries for a wide range of applications. However, it is mainly one-dimensional (1D) arrays with linear elements that are used. A consequence of using linear elements is that only two-dimensional (2D) slices of a component can be imaged at one time. This has the obvious drawbacks of potentially missing scattering from a defect in the out-of-plane direction, and the inability to accurately focus through surfaces that are curved in more than one direction, or 'doubly-curved' surfaces. A possible workaround for these issues is to implement 2D arrays, which have elements arranged across a 2D area. Similar to how linear elements in 1D arrays allow beam steering across a 2D plane, the element layout in 2D arrays permits beam steering throughout a three-dimensional (3D) volume without moving the array. This guarantees complete coverage of the imaging region, provided the array and surface orientations are favorable. The use of 2D arrays also enables 3D defect images to be obtained without combining a set of 2D images taken from different array positions. This is an important ability as defects can occur in arbitrary orientations in nature and accurately distinguishing between defect types and sizes is crucial for thorough inspections.

A current area of interest is the inspection of defects that are within regions where the surface is doubly-curved, as such those found in pipework branches and nozzles. There exists a number of methods to compensate for non-planar surfaces, but the method used here involves submersing the component in water in a scanning tank and extracting the surface using an imaging algorithm [1]. Due to the complex nature of this surface type, it is necessary for some surface inclinations to not have the array directly above the surface region to be imaged. This is required in order to obtain normal surface reflection of sound waves.

In this research, volumetric images of defects are obtained using a specimen with a doubly-curved surface. A 2D array is mechanically scanned over the surface and time-domain datasets are obtained at each array position in Full Matrix Capture (FMC) [2] format. The Total Focusing Method (TFM) imaging algorithm [2] is then used to produce images using each dataset. The images generated at each array position are combined into a single, larger image using a combining process termed 'stitching' here. The surface is then extracted from the stitched TFM image of the surface of the specimen and used to generate interior images of the specimen. The positioning of defects within the specimen is then investigated.

2. MATERIALS AND METHODS

2.1 Array and specimen

[1] Contact author: jessica.mckee@bristol.ac.uk

A previous study has showed that 2D arrays with elements arranged in a Poisson disc formation outperform a matrix array with the same number of elements [3], and therefore this type of array was used. The elements are circular in shape with a 1.7 mm diameter and minimum pitch of 1.9 mm. The array has a center frequency of 3 MHz.

The aluminum test specimen has a doubly-curved surface that is represented by a Gaussian profile with a steepest angle of inclination of approximately 24° relative to the horizontal. The specimen has 21 bottom-drilled holes (BDHs) of 3 mm diameter, and the tip of each hole is at a different depth below the surface. The specimen also has 4 electrical discharge machine (EDM) notches at different depths. A 3 mm hole is drilled into the surface of the specimen to act as a reference point for surface orientation and defect positioning. A side view illustration of the specimen is given in Figure 1(a), and the position of the defects on the base of the specimen is shown in Figure 1(b).

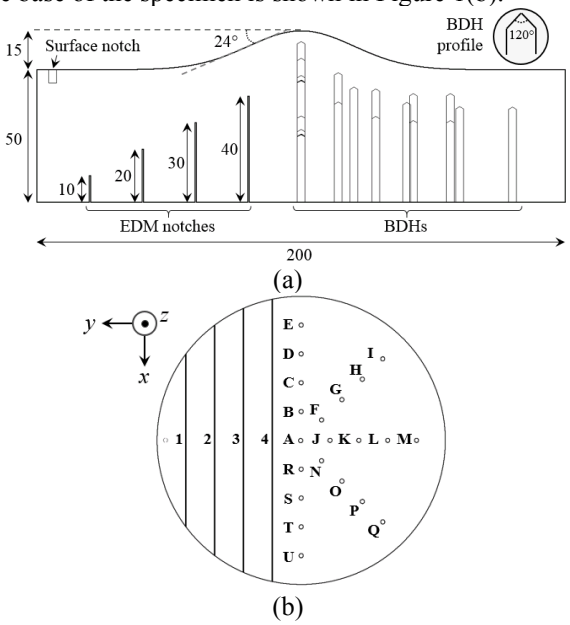

FIGURE 1: ILLUSTRATION OF THE DESIGNED SPECIMEN WITH MACHINED DEFECTS. (a) IS A SIDE PROFILE AND (b) IS A BASE VIEW.

2.2 Scanning procedure

The array was attached to a mount and raster scanned over the surface of the specimen in immersion in a scanning tank. The mount was connected to three motors to enable manipulation in the x, y, z directions. Before the scan, the array was aligned parallel to the back wall of the specimen over a flat surface region and moved to a standoff of 13 mm above the peak. The total scanned area was 240 x 240 mm^2 using a total of 225 array positions with a pitch of 15 mm in the x and y axes; the active area of the array was 30 mm so therefore the pitch resulted in a 50% array aperture overlap between array positions.

2.3 Image processing methods

As mentioned before, time-data at each array position was captured in FMC format and processed using a TFM algorithm. The entire imaging process is divided into three sections detailed below.

2.3.1 Surface imaging

An image of the surface of the specimen was required first in order to extract the surface profile, as its precise nature was unknown at this stage. This was achieved by implementing a single-medium TFM algorithm using each FMC dataset using only the velocity of sound in water, v_1. The time-of-flight (TOF) from each element to each image point in the imaging grid was found through basic trigonometry. For an arbitrary image point $\mathbf{P_1}$, the intensity, $I_{surf}(\mathbf{P_1})$, for each transmit-receive element combination was calculated using:

$$I_{surf}(\mathbf{P_1}) = \left|\sum h_{T,R}\left(\frac{\|\mathbf{E_T}-\mathbf{P_1}\|+\|\mathbf{E_R}-\mathbf{P_1}\|}{v_1}\right)\right| \qquad (1)$$

where the summation was over all transmit, T, and receive, R, element combinations. $h_{T,R}(t)$ represents the complex Hilbert transform of the time-trace corresponding to transmitting on T and receiving on R. Linear interpretation of $h_{T,R}(t)$ was required and $\|\cdot\|$ denotes the Euclidean norm of a vector.

When stitching the TFM images from each array position together, the maximum amplitudes of overlapping image points were taken as the true amplitudes. The result is a stitched single-medium 3D TFM image of the surface of the specimen.

2.3.2 Surface extraction

Due to the non-planar nature of the surface and the array orientation relative to the specimen, there was a variation of reflected signal strength. Simply taking the points of maximum amplitude resulted in a discontinuous and inaccurate surface so a more sophisticated surface extraction method was required. This involved applying depth constraints in the z-axis during the extraction process to ensure a continuous surface was obtained.

The starting point of the extraction process was the location of the image point with maximum amplitude in the stitched 3D surface TFM image. The 2D $(x-z)$ plane through this point was considered first. The two neighboring surface points were found by considering image points within the z-range $\alpha \pm \delta z$ where α is the z-coordinate of the starting point and δz is a small distance. The locations of the maximum amplitude in each z-range were taken as the next extracted surface points, as long as they exceeded an amplitude threshold. The process was repeated for the next neighboring points by replacing α with the most recently extracted z-coordinate until the edge of the surface was reached. The result of this step was an extracted 2D curve of surface points.

To obtain the 3D (x, y, z) coordinates of the extracted surface points, the process described in the previous paragraph was applied in the 2D $(y-z)$ planes through each of the extracted surface points along the 2D curve.

2.3.3 Interior imaging

A second set of TOFs between all elements and image points were calculated while considering the extracted surface points.

Fermat's principle of least time was used to determine the surface-crossing locations, **A** and **B**. The velocity of sound in the specimen, v_2 also needed to be taken into consideration in this stage. The intensity of the image, $I(\mathbf{P_2})$, at any image point in the interior imaging grid was calculated by summing over all T and R combinations using:

$$I(\mathbf{P_2}) = \left| \sum h_{T,R} \left(\frac{\|\mathbf{E_T} - \mathbf{A}\|}{v_1} + \frac{\|\mathbf{A} - \mathbf{P_2}\|}{v_2} + \frac{\|\mathbf{P_2} - \mathbf{B}\|}{v_2} + \frac{\|\mathbf{B} - \mathbf{E_R}\|}{v_1} \right) \right|. \quad (2)$$

Just like before, all interior TFM images from each array position were combined to create a stitched 3D TFM image of the interior of the specimen.

3. RESULTS AND DISCUSSION

The stitched 3D surface TFM image is shown in Figure 2 as an isosurface plotted at -10 dB relative to the maximum amplitude and colored according to z-depth. The RMS error between the true and extracted surfaces was 0.04 mm and the maximum absolute error was 0.20 mm.

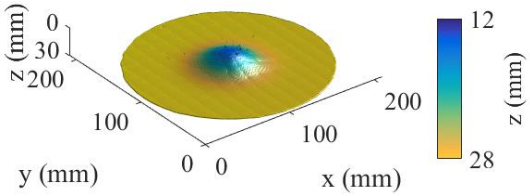

FIGURE 2: STITCHED 3D TFM IMAGE OF THE SURFACE.

The stitched 3D interior TFM image is shown as an isosurface at -28 dB relative to the back wall in Figure 3. Figure 3(a) shows the 2D $(y - z)$ plane with the 4 EDM notches located at (y > 115 mm) and the BDHs at (y < 115 mm). It was found that defects located under the steepest region of inclination were unable to be imaged as the surface inclination was greater than the critical angle for the water/aluminum boundary, which was 13.4°. For this reason, BDHs B, F, J, N and R are excluded from the results. BDH C is also excluded as the signal-to-noise ratio was too low for imaging.

The positioning of the defects was investigated by using two metrics. The first was the depth of each defect above the back wall, and the second was the lateral position of each defect from the surface notch. These distances were compared to the true values, with the depth and lateral results shown in Figure 4(a) and (b) respectively. The standard deviation of measurements corresponding to depth and lateral position is 1.16 mm and 0.97 mm respectively.

4. CONCLUSION

The use of FMC and TFM have demonstrated the ability of 2D phased arrays to accurately image defects through doubly-curved surfaces. A stitching method was implemented to combine many individual datasets taken from different positions and the surface was extracted within an absolute error of 0.07 mm. While the visible defects were able to be accurately positioned, the defects that are located under the steepest inclined region were not able to be imaged.

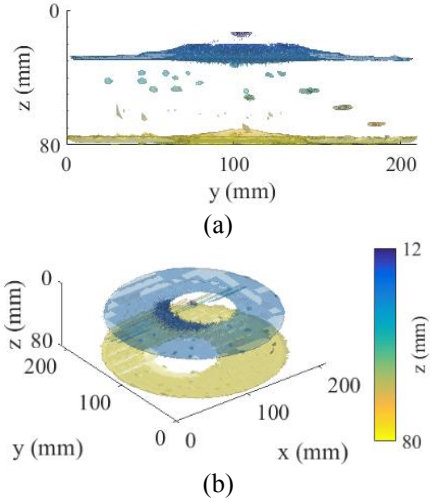

FIGURE 3: STITCHED 3D TFM IMAGE OF THE INTERIOR OF THE SPECIMEN.

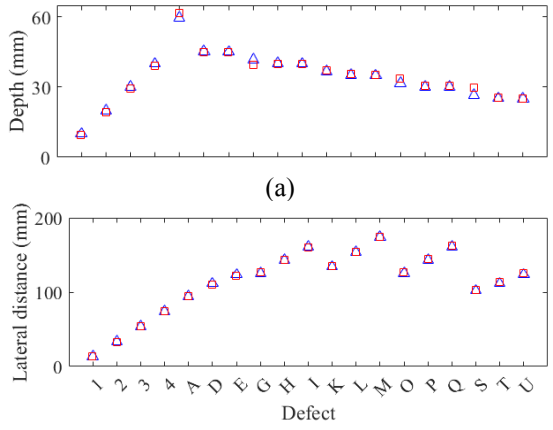

FIGURE 4: COMPARISON OF TRUE (TRIANGLE) AND MEASURED (SQUARE) DEFECT POSITIONS.

REFERENCES

[1] Malkin, Robert E., Franklin, Amanda C., Bevan, Rhodri L.T., Kikura, Hiroshige and Drinkwater, Bruce W. "Surface reconstruction accuracy using ultrasonic arrays: Application to non-destructive testing." *NDT&E International* Vol. 96 (2018) pp. 26–34. DOI 10.1016/j.ndteint.2018.03.004.

[2] Holmes, Caroline, Drinkwater, Bruce W. and Wilcox, Paul D. "Post-processing of the full matrix of ultrasonic transmit–receive array data for non-destructive evaluation." *NDT & E International* Vol. 38 (2005) pp. 701–11. DOI 10.1016/j.ndteint.2005.04.002.

[3] Velichko, Alexander and Wilcox, Paul D. "Defect characterization using two-dimensional arrays." *Review in Progress of Nondestructive Evaluation* Vol. 30 (2011) pp. 835–842. DOI 10.1063/1.3591934.